Atomic Defects and Their Relationship to Aragonite–Calcite Transformation in Portlandite Nanocrystal Carbonation

ARTICLE *in* CRYSTAL GROWTH & DESIGN · OCTOBER 2012

Impact Factor: 4.89 · DOI: 10.1021/cg300628m

CRYSTAL GROWTH & DESIGN

Article

pubs.acs.org/crystal

Atomic Defects and Their Relationship to Aragonite–Calcite Transformation in Portlandite Nanocrystal Carbonation

L. S. Gomez-Villalba,* P. López-Arce, M. Alvarez de Buergo, and R. Fort

Instituto de Geociencias (CSIC-UCM), Jose Antonio Novais 2 Str, 28040 Madrid, Spain

ABSTRACT: The defects in calcium carbonate polymorphs forming when portlandite nanocrystals are exposed to high relative humidity were directly observed and analyzed under high-resolution transmission electron microscopy. The findings provided significant insight into aragonite to calcite phase transformation mechanisms. The aragonite lattice exhibited stacking faults, the insertion of extra atomic planes into its normal sequence, and vacancies. These defects were shown to generate minor lattice translation of around $1/3d_{111\text{aragonite}}$ or nanovoids $2d_{111\text{aragonite}}$ or $3/2d_{020\text{aragonite}}$ in size. The presence of both extra atoms and nanovoids suggests the involvement of crystallization/dissolution processes. Calcite phase nucleation transformation mechanisms were observed as a result of the rearrangement of CO_3^{2-} anions in areas characterized by the disorder resulting from aragonite lattice dislocations. A series of dislocations, stacking faults, and modulated microstructures were identified in the neoformed calcite nanocrystals, more intensely after shorter than after longer exposure times.

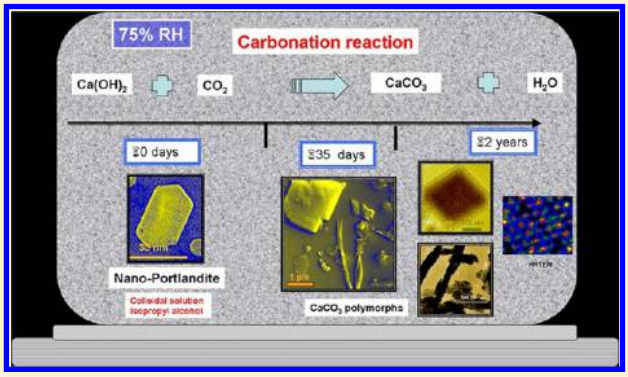

INTRODUCTION

Calcium carbonate ($CaCO_3$) is one of the most abundant naturally occurring neutral oxysalts. The main component of most carbonate rocks, it also forms the skeleton of a host of organisms. Given its structure and composition, it is commonly used in a number of industries: medicine and pharmaceuticals, construction, and oil, to name a few.

$CaCO_3$ may adopt the form of anhydrous (calcite, aragonite, and vaterite) or hydrated oxysalts (monohydrocalcite, ikaite, and the amorphous variety of $CaCO_3$, ACC).

Calcite (JCPDF = 83-1762, a = 4.989 Å, c = 17.06 Å, $R\bar{3}c$) and aragonite (JCPDF = 76-0606; a = 4.959 Å, b = 7.964 Å, c = 5.737 Å, *Pmcn*) share certain crystallographic properties. Both derive from close packed structures, cubic in the case of calcite and hexagonal in aragonite. The two structures are thus closely related in terms of phase transformations.[1] The crystalline structure of aragonite differs from the calcite skeleton only in that its hexagonally packed Ca^{2+} and CO_3^{2-} ions are denser. The coordination number for the cations in the calcite rhombohedral network is six, and that in the aragonite network is nine.[2]

Transformation from unstable aragonite to more thermodynamically stable calcite has been widely studied in the context of $CaCO_3$ transformation to CaO when heated.[3,4] This transformation has likewise been analyzed in biomineralization processes,[5,6] including aragonite replacement by calcite.[7−9] They have inspired the design of certain man-made nanostructural compounds.[10−12]

Significant progress has been made in the determination of certain structural defect-related characteristics of these crystals. Most of the studies in question were conducted on $CaCO_3$ samples from geological or biological materials.[1] Barber[13] and Guderson and co-workers,[14] provided a wealth of in-depth information on the structural details of $CaCO_3$ (calcite) and $CaMg(CO_3)_2$ (dolomite).[15] Those studies were limited by the resolution of the microscopes used, however.[16] Therefore O'Keefe and Barber[16] suggested the use of 2.5 Å point-to-point resolutions to determine the presence of Ca cations, 1.7 Å resolutions for CO_3 anions, and 1.3 Å resolutions for oxycarbons.[17] Moreover, while structural findings have led to a more detailed understanding of the atomic behavior of calcite,[18−21] as well as of aragonite albeit to a much lesser extent,[9,22,23] little is known about the nucleation and growth of these polymorphs under conditions other than those used to study natural mineral or biological materials.

$CaCO_3$ may be obtained when calcium hydroxide ($Ca(OH)_2$, portlandite) is exposed to atmospheric carbon dioxide (CO_2) and high relative humidity (RH). The layered hexagonal crystalline network in portlandite favors the intake of CO_2. The concomitant release of H_2O induces carbonation, with the conversion of $Ca(OH)_2$ into several calcium carbonate polymorphs. The main physical–chemical processes involved in portlandite carbonation are CO_2 diffusion at the gas/liquid interface, CO_2 dissolution in water to form carbonic acid (H_2CO_3), its dissociation into HCO_3^- and CO_3^{2-} ions, the dissolution of $Ca(OH)_2$, the release of Ca^{2+} ions and OH^- groups, and last Ca^{2+} and CO_3^{2-} precipitation, forming $CaCO_3$

Received: May 9, 2012
Revised: July 30, 2012
Published: August 21, 2012

   dx.doi.org/10.1021/cg300628m | *Cryst. Growth Des.* 2012, 12, 4844–4852

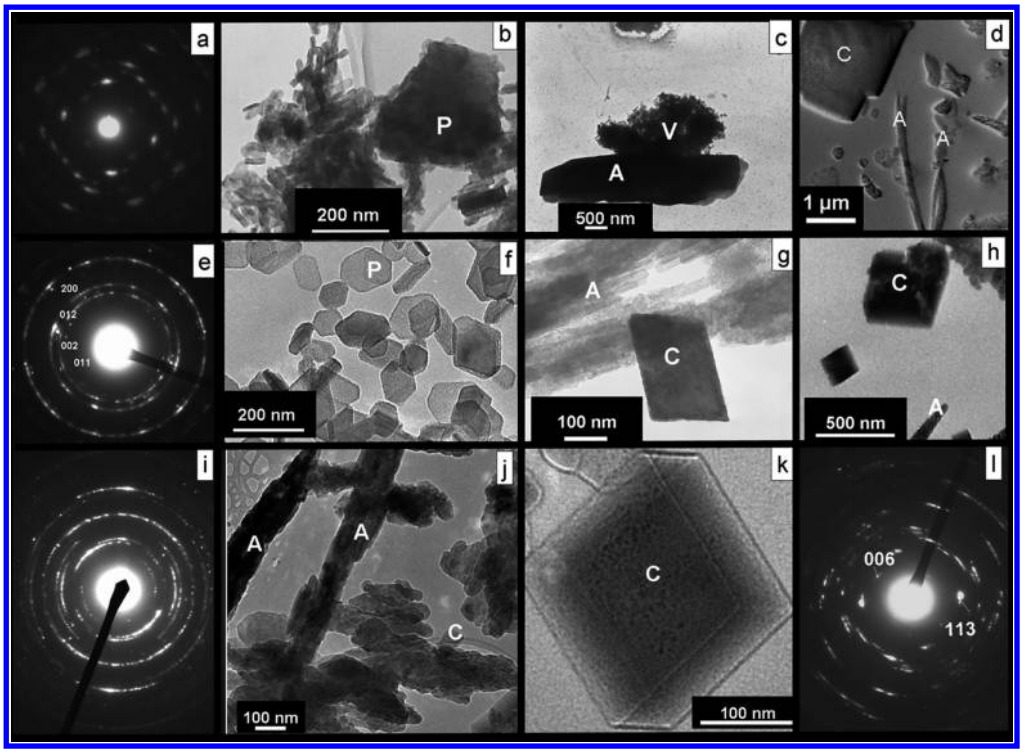

Figure 1. SAED patterns (a, e, l, and i) and low-magnification TEM images (b–d, f–h, j, k) in bright field mode for solutions exposed to 75% RH: (a) SAED pattern for solution A, 0 days; (b) solution A, 0 days; (c) solution A, 14 days; (d) solution A, 35 days; (e) SAED pattern for solution B, 0 days; (f) solution B, 0 days; (g) solution B, 14 days; (h) solution B, 35 days; (i) SAED pattern for solution A, 14 days; (j) solution B, 2 years; (k) calcite crystal in solution B, 2 years; (l) SAED pattern for solution B, 35 days. P, portlandite; V, vaterite; A, aragonite; C, calcite.

and releasing H_2O.[24] This reaction is controlled, among others, by the partial pressure of CO_2[25] and pH.[26]

The carbonation reaction has been studied for different purposes of late, one being the determination of its role as a consolidant that restores cohesion in weathered rocks.[27,28] $CaCO_3$ stability is conditioned by relative humidity and the duration of the exposure to the environmental conditions in which carbonation takes place, among others. An analysis of some of these reactions in nanoportlandite solutions has shown that carbonation kinetics are faster in moist than in dry environments.[29,30] The effect of the precursors used and the specific conditions for preparing the solution (mechanical or ultrasonic stirring) have also been studied to determine the conditions in which $CaCO_3$ is formed. In a specific case reported by López-Periago,[31] the presence of a large amount of liquid water was found to lead to the precipitation of micrometric particles, whereas when less water was available, calcite precipitation was nanometric.

The present study is based on research conducted to monitor spontaneous carbonation in two portlandite nanocrystal colloidal solutions dissolved in isopropyl alcohol. Prior carbonation studies[29,30] showed that carbonation and differences in polymorph nucleation and stability depend heavily on relative humidity.[32] The presence of alcohol in binary alcohol–water mixtures can affect the precipitation pathway of anhydrous crystalline $CaCO_3$ polymorphs and their morphology.[33] According to the aforementioned studies, local variations in the water/alcohol ratio have a significant impact on their precipitation and dissolution, and all these factors are mirrored in crystal growth. Changes in lattice parameters and particle size are related to fluctuations in surface tension and the release of residual water during carbonation. The differences in polymorph lattice parameters show that cell parameters are greater at high than at low relative humidity and decline with exposure time at any given humidity value.[30,32] In the aforementioned studies, polymorph crystallinity attained at 75% RH was compared with the values observed at 90%, 54%, and 33% RH. At the lower two values, carbonation was very slow and practically nonexistent at 33% after 1 month exposure. At low RH, carbonation was observed to begin with portlandite amorphization and amorphous carbonate nucleation. In that case, the excess alcohol in the solution reduced the surface tension, and nucleation was affected by speedy solvent evaporation, which prevented the particles from diffusing to lower energy sites during evaporation. The outcome was smaller particles and a lower degree of crystallinity.[32]

These results are applicable to biomineralization processes as well, since most micro-organisms excrete alcoholic solutions, which in aqueous environments may lead to modifications in crystallinity or phase changes similar to the results obtained with this experimental procedure.

The pharmaceutical industry has conducted research geared to determining the sensitivity of carbonates to changes in relative humidity.[34] The study of their hydrophilic behavior revealed RH-related solubility differences that may be associated with structural defects.

The primary aim of the present paper is to establish the relationship between atomic scale structural defects and mechanisms that may be related to aragonite to calcite (hereafter aragonite–calcite) phase transformations observed after lengthy exposure of nanoportlandite to high (75%) relative humidity. The results obtained are of great interest to a number of research groups, most of which are working on the determination of crystallographic orientations in nascent

dx.doi.org/10.1021/cg300628m | *Cryst. Growth Des.* 2012, 12, 4844–4852

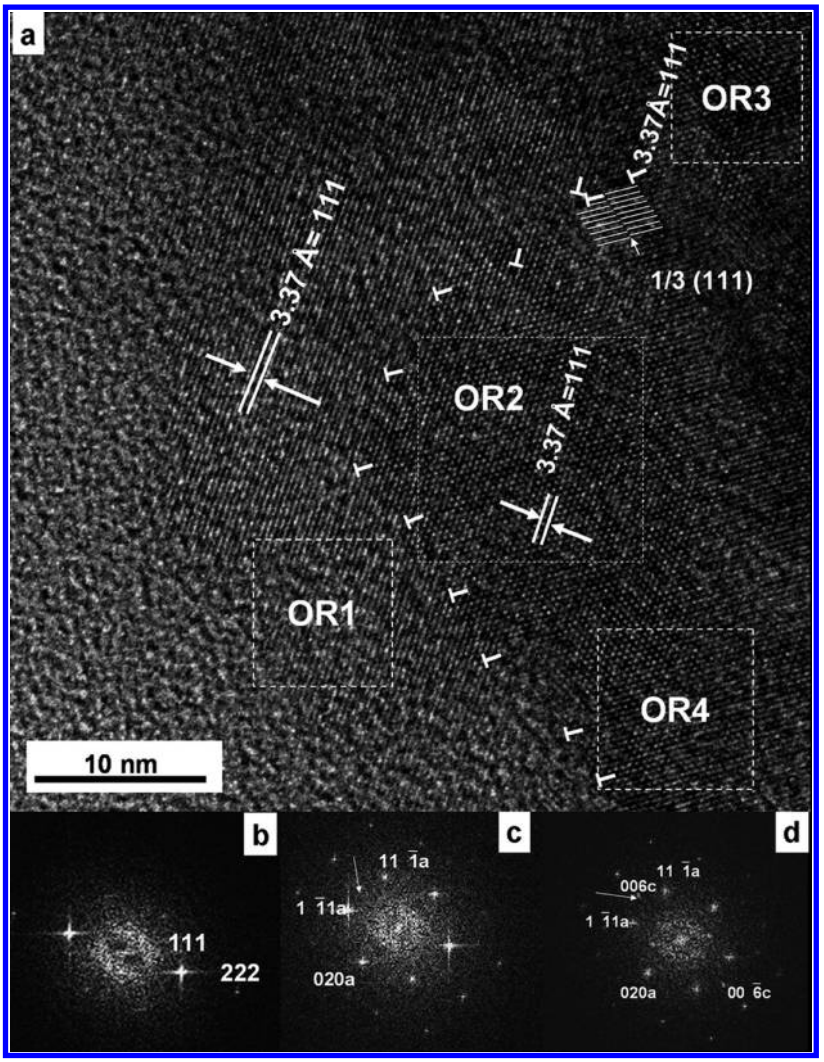

Figure 2. (a) HRTEM for 35 day aragonite (solution A); fft for (b) OR1, (c) OR2, and (d) OR3.

$CaCO_3$[1,9] or the durability and conservation of carbonated products.

MATERIALS AND METHODS

Experimental Section. Two colloidal solutions of hexagonal plate-like $Ca(OH)_2$ nanocrystals dispersed in isopropyl alcohol were used in this study: Nanorestore (sample A) and CaLoSil (sample B). Both were subjected to additional ultrasonic dispersion in a 5-min ultrasonic bath (Selecta Ultrasounds-H). A drop of each precursor solution was placed directly on a copper grid coated with a fomvar-type resin for TEM analysis. The samples were then stored inside a closed desiccator used as a climatic chamber and exposed to 75% relative humidity (RH) at 20 °C for 14 or 35 days or 2 years. The concentration of CO_2 in the room, measured with a CO_2 detector (Ventostat8002, Telaire, Goleta, CA, USA), was approximately 550 ± 50 ppm. No additional flow of CO_2 was present nor was the air in the chamber allowed to circulate.

The equilibrium relative humidity (RHeq) of a supersaturated NaCl solution was used to ensure a high and constant RH (RHeq 75%) at 20 °C in the desiccator. The salt was set inside a container at the bottom of the chamber. The copper grid holding the nanoparticles was positioned several centimeters above the supersaturated salt solution to ensure that the salts never physically touched the nanoparticles. A RH sensor (Onset Hobo data logger) was used to monitor the desirable RH and temperature in each chamber, in turn located in an environment where the conditions recorded were 76.8% ± 4.3% at 18 ± 2 °C.

Microscopic Analysis. The samples were first viewed under low-magnification TEM in bright field mode, combined with selected area electron diffraction (SAED). Subsequently, a high-resolution transmission electron microscopic (HRTEM) study was conducted in conjunction with Fourier filtering (fast Fourier transform (fft) and inverse fast Fourier transform (ifft)) to identify atomic scale defects and relate them to aragonite−calcite phase transformation. The Fourier filtering method, equivalent to electron diffraction, was used to avoid the risk of phase transformation induced by the long exposure to the electron beam required in electron diffraction and to detail on smaller areas. The instrumental conditions were as follows: JEOL-JEM 3000 electron microscope, 300 kV, 1.7 Å point-to-point resolution, image mode. Short exposure times of only a few seconds were used to protect the sample from decarbonation caused by calcium carbonate radiolysis.[35,36] Digital Micrograph software was used to analyze HRTEM images.

Conventional TEM and SAED analyses were conducted on the two starting solutions, as well as on the 14 and 35 day and 2 year samples stored at 75% RH. Based on the results of prior research,[29,30] postcarbonation crystallinity was studied by HRTEM in the 35 day and 2 year samples. Since such studies can only be run on samples thin enough to be penetrated by an electron beam, 2 year HRTEM imaging was conducted on the solution B samples only. The software used for the crystallographic study included Electron Diffract, Visualization for Electronic and Structural Analysis (VESTA, version 1.3.0)[37] and Jmol, version 11.4.0. The statistical analysis was run with Dip software.

dx.doi.org/10.1021/cg300628m | Cryst. Growth Des. 2012, 12, 4844−4852

RESULTS AND DISCUSSION

Low Magnification Observations. Crystallographic differences were observed between the two solutions during carbonation, which were visible in the low-magnification TEM images and respective SAED patterns.

Zero-Day Samples. In both cases, the starting solution contained portlandite crystals, which differed in habit, degree of aggregation, and particle size. Clusters of plate-like nanocrystals (60−400 nm) were observed in solution A (Figure 1b), whereas in solution B the nanocrystals (60−130 nm) were hexagonal and disaggregated (Figure 1f). The electron diffraction patterns also exhibited slight differences. While the textured SAED pattern observed for solution A suggested significant proportions of structural defects (Figure 1a), the pattern for solution B (Figure 1e) showed more continuous polycrystalline rings with fewer defects.

Fourteen Day Samples. Vaterite (V) and aragonite (A) polymorphs nucleated in both solutions, although certain differences were observed in their crystalline habits (Figure 1c, solution A, and Figure 1g, solution B). The crystalline habit for the aragonite was slightly more fibrous and aggregated in solution B than in solution A (Figure 1g,c). The highly textured SAED pattern shown here for solution A (Figure 1i) suggested a high proportion of crystalline defects.

Thirty-Five Day Samples. The calcite habit differed in the two solutions, although the compound was associated with needle-like aragonite crystals in both. Figure 1d shows a 2 μm calcite crystal identified in solution A, associated with acicular aragonite crystals (>3 μm), while 200 and 600 nm calcite was observed in association with aragonite needles in solution B, as illustrated in Figure 1h. The SAED pattern for calcite (Figure 1l) suggested a high defect content.

Two Year Samples. A rhombohedral calcite crystal (~200 nm) (Figure 1k) was identified in solution B among the aragonite needles. Note that the aragonite crystals were very large compared with their calcite counterparts (Figure 1j). Since crystal size and thickness in 2 year solution A were too large to obtain TEM images suitable for a high-resolution study, only the images for solution B are shown here.

The morphological and structural differences in the two starting solutions (Figure 1b,f) are indisputably the predominant factors in the morphostructural characteristics of the future polymorphs and the development of point defects. Such defects act as embryos for possible subsequent epitaxial growth that may appear at any time during carbonation. Aquilano et al.[38] showed that crystal morphology is affected by a number of factors, including most prominently the substrate on which the solutions are deposited and the relative humidity in the surrounding environment. In this case, however, the solutions were deposited on the same resin, used for TEM observation, and exposed to the same relative humidity and CO_2 concentration for the same amount of time. Other factors that should be taken into consideration, then, include the differences in the conditions in which the two colloidal solutions were synthesized (variations in experimental parameters, that is, type of precursors, additives, solvents, and preparation time) or the effect of short-range properties such as solvent absorption[23] or surface tension fluctuations.[30] The differences observed in crystal growth between the unstable polymorphs (aragonite and vaterite) are the result of Ostwald ripening.[30] Moreover, crystallinity was affected by variations in energy during the carbonation reaction.[30] Detailed morphological and structural analyses using other characterization techniques are available for both solution A[29] and solution B.[30]

High-Resolution Study. *Thirty-Five Day Aragonite.* Figure 2a shows the lattice image of 35-day aragonite crystals (solution A), and the respective optical diffractions for several ordered regions (OR) identified on the image are shown also (Figure 2b, OR1; Figure 2c, OR2; Figure 2d, OR3). The orientation in OR1 is such that the 111 systematic reflections in the optical diffraction pattern (Figure 2b) generate 3.37 Å fringe spacing. The grain boundary with OR2 is delimited by a dislocation array. OR2 and OR3 differ in the atomic arrangement oriented along the $[10\bar{1}]$ zone axis. Atomic planes 111 and 020 show a slight rotation ($\theta = 2.69°$). A minor lattice translation of around $1/3d_{111}$ induces displacement in the stacking sequence. Some of the satellite reflections (arrows in Figure 2c,d) suggest the presence of other lattice defects in the stacking sequence.

The stacking sequence in OR3 (Figure 3a) is disrupted by the presence of nanovoids of up to $2d_{111\text{aragonite}}$ or $3/2d_{020\text{aragonite}}$

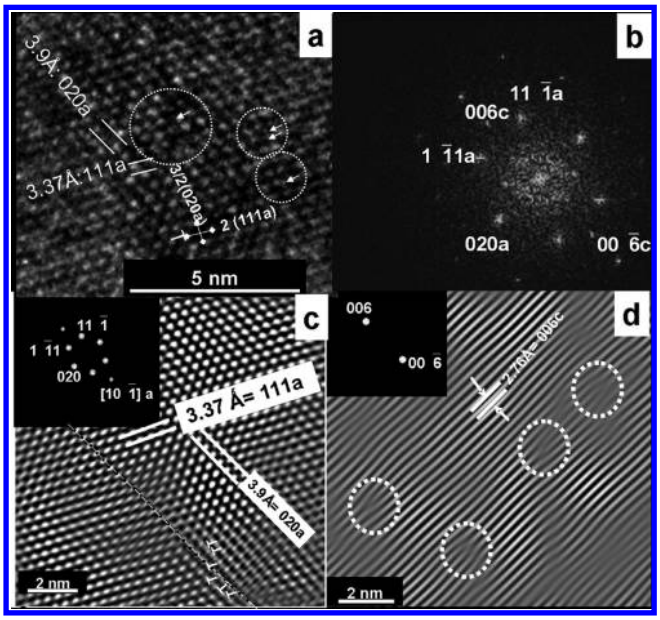

Figure 3. Details of OR3 (solution A): (a) extra atoms (circles) and nanovoids in the aragonite stacking sequence; (b) fft indexed along $[10\bar{1}]$ aragonite where the extra spots are calcite reflections; (c) ifft image showing the contribution of aragonite only from fft (insert); (d) ifft image with the contribution of calcite {0006} reflections only from fft (insert).

and by a series of extra atoms (circles). The respective fft (Figure 3b) shows arrays of spots pertaining to $[10\bar{1}]_{\text{aragonite}}$, although other additional spots are consistent with the atomic distance for $d_{0006\text{calcite}}$. The image was studied by ifft to identify the defects associated with the two atomic lattices. Two ifft images were consequently calculated. The image shown in Figure 3c, obtained using only one set of $[10\bar{1}]_{\text{aragonite}}$ parallel Fourier spatial frequencies, shows curved rows of atoms in which $d_{020\text{aragonite}}$ and $d_{111\text{aragonite}}$ are resolved. This curvature in the lattice planes is commonly a result of edge dislocations.[39] The ifft image in Figure 3d was obtained by selecting only the additional spots attributable to $d_{0006\text{calcite}}$ atomic columns, although these atoms also are subject to dislocation. The circles indicate the positions where three misfit dislocations meet. On the grounds of defect distribution and dislocation cores, these

dx.doi.org/10.1021/cg300628m | Cryst. Growth Des. 2012, 12, 4844−4852

structures can be attributed to the insertion of extra atomic planes and vacancies into the normal sequence in the aragonite lattice.

While several authors have reported porosity as well as stacking faults after long exposure times to an electron beam, defects pre-existing in the aragonite crystal have also been reported to favor phase change. A certain degree of porosity along the edges of the aragonite grains was reported in several papers, such as in the transformations in carbonatite rock in natural marine environments,[1] in the exoskeletons of certain organisms,[1] or in experimental studies under hydrothermal conditions.[40] Such microporosity was associated with dissolution, which contributes to the generation of defects that affect nucleation and growth during aragonite−calcite replacement.[1]

The HRTEM image also reveals certain anion and cation characteristics. The differences in contrast visible in Figure 4a provide information on the distribution of Ca^{2+} and CO_3^{2-} ions. The bright spots are Ca^{2+} atoms, while the low scattered dots denote the presence of CO_3 layers. Certain differences related to the periodicity of atomic planes can be observed in Figure 4a. At left and center, the image depicts an aragonite-type domain, oriented in the [10$\bar{1}$] direction (confirmed in the fft, upper right), while at the right it shows a characteristic calcite-type domain, where the atomic planes resolved have a periodicity equivalent to d_{0006}. The cation sequence in the aragonite plane was observed to be interrupted by point defects, leading to stacking faults, slight dislocations, or extra atoms. These point defects are labeled in the image with Burgers vectors and circles.

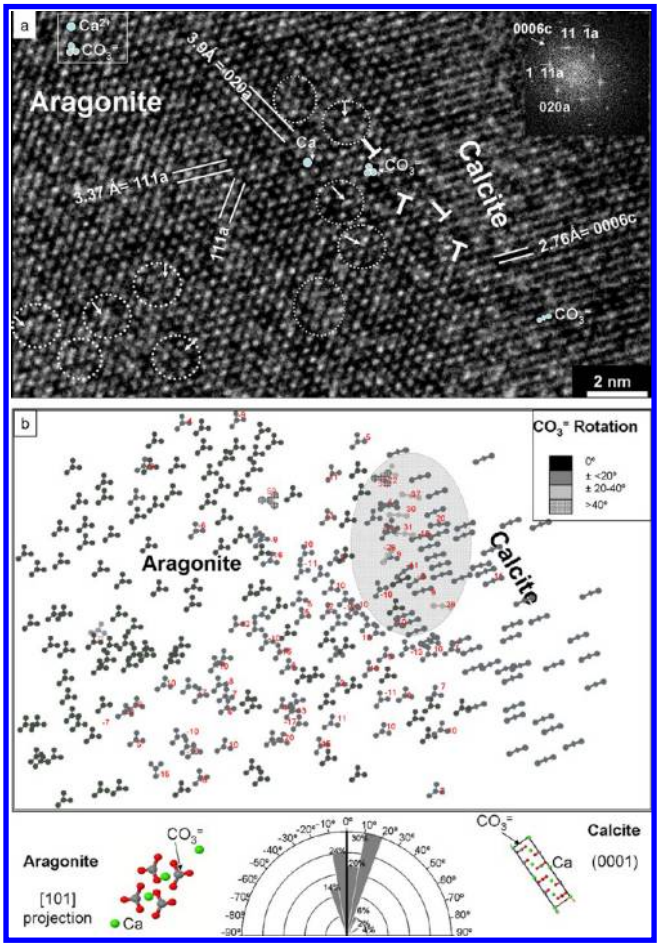

Figure 4. (a) HRTEM image showing two crystalline domains, aragonite (left) and calcite (right), with point defects (circles); bright spots correspond to Ca^{2+} cations. Inset shows the respective fft (solution A). (b) (top) distribution of CO_3^{2-} anions (symbolized as triangles) as viewed in the image in panel a; (bottom) (left) general model for aragonite along its [101] axis zone; (right) general model for calcite along its plane 0001; (center) rosette diagram showing anion rotation statistics for both aragonite and calcite.

Figure 4b is a schematic drawing of the anions in the HRTEM image, depicting their rotations. Taken as a whole, the CO_3^{2-} group resembles an equilateral triangular with oxygen atoms at the corners and a carbon atom in the center.[41] The CO_3^{2-} anions in Figure 4 are consequently symbolized by triangles for readier interpretation given that the resolution of the instrument used was insufficient to differentiate between oxygen and carbon atoms. While the present study does not aim to develop theoretical models for anion and cation distribution, certain characteristics in this regard can be identified on the experimental image. The theoretical models proposed for aragonite[42] in the [101] zone axis and for calcite[43] along plane (0001) are shown in the lower left and right, respectively, of Figure 4b. Both structures consist of alternating Ca^{2+} and CO_3^{2-} layers.

The behavior of the anions in the "aragonite-type environment" (to use Parsonage and co-workers'[2] term) (Figure 4b) denoted progressive left to right rotation, reaching values of up to 20° and 35° both clockwise and counter-clockwise, in the transition zone (shaded). The actual rotation values for each anion resolved in the HRTEM image are shown in Figure 4b. Anion rotation reached values of around 50° in the "aragonite-type environment", concurring with the presence of extra calcium atoms (see Figure 4a). The "calcite-type environment" anions, running parallel to 0006, exhibited only slight rotation in some of their outermost layers, with values from 11° to 29°. CO_3^{2-} ion behavior differed across the "calcite-type environment" in the shaded area in Figure 4b, where plane 0006 predominates. Here, the most intense rotation (±29−30°) was observed in the anionic columns positioned in the upper part of the area closest to the aragonite domain, although values as low as 10° were also detected. The behavior observed in the lower right differed substantially, for no rotation took place, with anions spreading across the plane laterally. The rosette diagram in the lower part of the figure summarizes the anion rotation statistics for the two crystalline domains, with rotation angles of ±10−20° prevailing in both.

The surface reconstructions and relaxation effects studied by Bruno and co-workers[19] on $(00.1)^{Ca}$ and $(00.1)^{CO3}$ (authors' notation) surface structures in a centrally symmetrical calcite crystal provide useful insight into ionic behavior. The authors performed two types of reconstructions and reported on the equilibrium geometry of Ca^{2+} and CO_3^{2-} ions in the outermost layer, obtained with the force field method. Each adjacent pair of Ca^{2+} and CO_3^{2-} layers, d_{006} thick in all, was denominated a slice. The calculations performed for the unrelaxed and relaxed structures in each slice (in one of the reconstructions) showed that cations and anions were not equally distorted, for the latter exhibited lower relaxation. Moreover, ionic distortion even varied between slices from the same slab. More specifically, they reported that "the first slice of the $(00.1)^{Ca}$ slab was more compact than the layers underneath it, since the Ca ions and the centers of mass of the CO_3 anions tend to settle on a common plane. Relaxation mainly affects the five upper slices of

dx.doi.org/10.1021/cg300628m | Cryst. Growth Des. 2012, 12, 4844−4852

the slab. In slab $(00.1)^{CO3}$, the four uppermost slices were perceptibly rearranged, with the most intense CO_3 ion rotation observed in the second slice of the slab. In the anionic and cationic slices, the CO_3 groups were rotated around both the [010] axis and in the [001] directions." (For a fuller description, see Bruno and co-workers.[19])

Pursuant to Bruno and co-workers'[19] well-suited model, the anion behavior observed in the present study may be assumed to be very similar to the description of a relaxed structure such as calculated for calcite along plane 0006. The existence of point defects in the atomic network (more readily observed in cations), whose presence is favored by the action of environmental water (Figure 4), must also be taken into consideration, however. Indeed, in the present study the crystals were grown under controlled laboratory conditions and their surfaces were constantly exposed to high relative humidity. Although correlating the findings from surface reconstructions to the experimental results of grown crystals lies outside the scope of the present study, no doubt can be harbored about the importance of such calculations or of the variables involved.

For aragonite, Aquilano and co-workers[23] contributed to an understanding of theoretical equilibrium as well as growth morphology along {110} and {010}, which form part of the [001] zone axis. Their study addressed the essential role played by crystal surfaces in contact with the growth medium in the determination of equilibrium shapes, nucleation frequencies, and epitaxial interfaces during polymorphic transitions, among others. These authors[23] showed that stacking in the [001] direction in crystal growth units is the grounds for pseudohexagonality and explained the ready growth of aragonite crystals when twinning on [110].[23] In the aragonite-type anion behavior depicted in Figure 4, progressive rotation would be expected in a transition zone between two crystalline domains. In the present experimental study (in which the crystalline aggregates were grown on a substrate), however, the CO_3^{2-} rotation in the aragonite−calcite transition zone that affects the aragonite 111 and 020 planes on the [101] zone axis was not progressive but in fact abruptly interrupted by point defects. As the HRTEM images show, the presence of point defects, stacking faults, or dislocations in general favor reaccommodation of both cations and anions, interrupting progressive ionic rotation. Such rotation is more readily visible in the experimental image, which depicts the behavior of the CO_3^{2-} anions. Another interesting observation is that no twinning defects were identified in the [101] direction.

The progressive loss of reflections attributed to anion ordering has been proposed as a sign of aragonite−calcite transformation.[3] Carlson and co-workers[3] observed that calcite grains saturated aragonite grain boundary surfaces, cleavage traces, and fracture surfaces in natural rocks. Calcite crystals invariably adopted specific orientational relationships relative to the aragonite structure. The most common orientations observed were the ones for which a very high degree of coherence between the two structures could be maintained and for which Ca-atom sites in the two superimposed lattices coincided most closely. These observations may be interpreted to conclude that calcite nucleation in natural occurrences takes place to reduce interfacial strain and misfit energies to a minimum, thereby lowering activation energies and increasing nucleation rates.[3] In addition, calcite recrystallization has been determined primarily on the grounds of crystal defects, suggesting that replacement kinetics are governed primarily by aragonite microstructure.[44]

Barber and Wenk,[15] studying $CaMg(CO_3)_2$ ($R\bar{3}$ symmetry), described changes in the structure of the CO_3 sublattice and additional reflections consistent with the presence of a second phase as indicators of disorder. The glide of dislocations were found to generate dislocation interactions that disturbed the regular arrangement of CO_3^{2-} groups.

Two of the several mechanisms proposed for aragonite−calcite transformation are the topotactic mechanism and the dissolution/recrystallization process. In previous TEM studies, dissolution/precipitation processes were described in which carbonate precursor and end product coexisted.[17] Frisia-Bruni[44] however reported the presence of both topotactic and nontopotactic replacement. In aragonite, replacement may occur preferentially along twin boundaries. Experiments conducted in a number of aqueous environments led to the conclusion that when precipitation takes place in voids in primary or secondary porosity, calcite nucleates heterogeneously, often as epitaxially oriented overgrowths; in situ replacement often generates calcite grains whose orientation and morphology are controlled by the aragonite precursor. The strong tendency for calcite nuclei to form in close crystallographic association with pre-existing crystals is a readily predictable consequence of the reduction in activation energy afforded by heterogeneous nucleation and by orientations yielding low-energy interfaces.[3]

Dissolution/precipitation events can be inferred from the coexistence of the two nucleated polymorphs, which have different morphologies and sizes, along with the presence of nanovoids, stacking faults, vacancies, and extra atoms. Those processes entail dissolution of the (unstable) parent phase and nucleation and growth of the (metastable or stable) daughter phase.[45] Assuming topotactic transformation (i.e., where parent and daughter phases have a sufficiently large proportion of structures in common), the solid state transformation mechanism would maintain the size and approximate shape of the parent phase. The dissolution/crystallization mechanism, by contrast, might involve morphological variations.[45]

Thirty-Five Day Calcite. The 35-day calcite generated in solution A at 75% RH (Figure 5a, low-magnification TEM image) consisted of a crystal (280 nm) having a surface with densely arranged 20−42 nm elongated domains and sinusoidal dislocations (arrows). An analysis of very thin crystals revealed differences in crystallinity. The outermost region (OR1, Figure 5b, low-magnification HRTEM image) constituted an amorphous edge (~20 nm wide) adjacent to a thin region with one elongated crystalline domain (OR2). Enlargement (of the framed area) revealed a modulated structure affecting the {0006} atomic planes.

The inner region parallel to the modulated area (OR3, Figure 5d, HRTEM image) was more crystalline, and a $11\bar{2}0$ reflection appeared. It contained relatively few defects, most of them fairly low-density dislocations whose cores (circles) affected atomic planes 0006 and $11\bar{2}0$. A number of stacking faults caused local displacements with spacing of around $1/3d_{0006}$.

Mosharraf and co-workers[34] theorized that their solubility test, differential scanning calorimetry, and density measurement findings for calcium carbonate particles exposed to high relative humidity were indicative of the presence of a disordered or amorphous layer on particle surfaces. The decline in apparent solubility of the compound after storage at high relative humidity indirectly suggested that recrystallization was taking

dx.doi.org/10.1021/cg300628m | Cryst. Growth Des. 2012, 12, 4844−4852

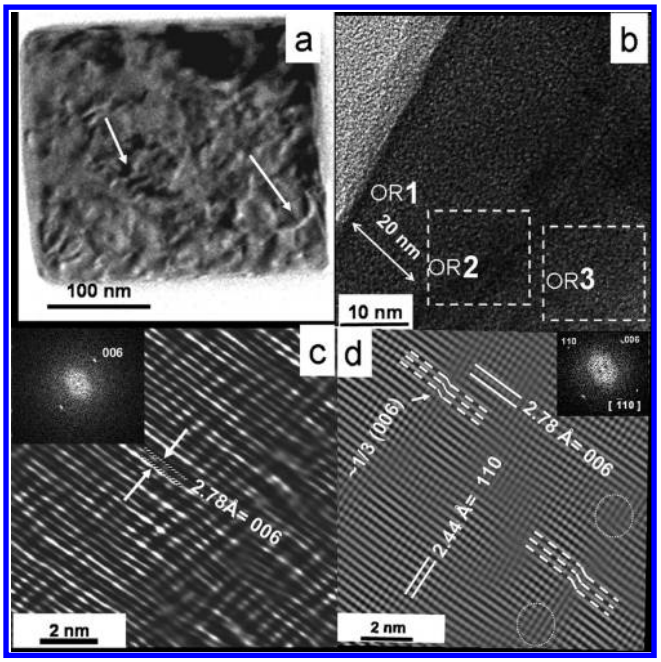

Figure 5. Calcite crystal in solution A after exposure to 75% RH for 35 days: (a) low-magnification TEM image; (b) low-magnification HRTEM image; (c) HRTEM-fft for OR2; (d) HRTEM-fft for OR3.

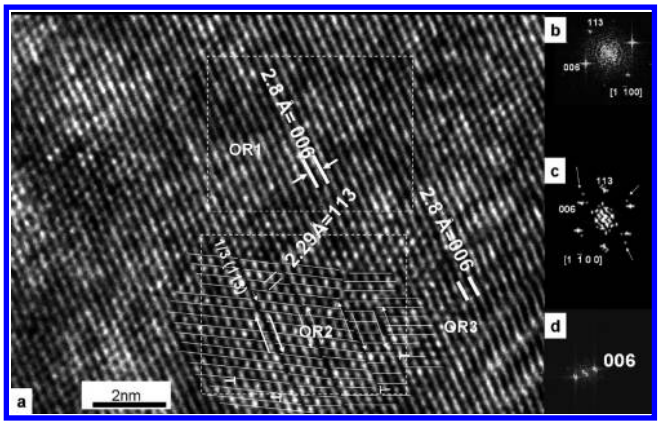

Figure 6. (a) HRTEM of a rhombohedral calcite crystal after 2 years exposure to 75% RH (solution B); fft for (b) OR1, (c) OR2, and (d) OR3.

place very slowly. The authors surmised that the reason for such slow recrystallization might be that the thin molecular layer of the particle surfaces that was in contact with the vapor inside the desiccator may have reached equilibrium, while their inner cores remained intact and substantially unaffected by the environment.[34] Moreover, disordered materials have been shown to absorb water vapor and recrystallize when stored in high relative humidity environments.[46]

Wenk and co-workers[1] identified modulated structures in calcium dolomites that clustered for formation during the growth process. They also reported that when calcite replaces aragonite, it may display a pervasive modulated structure. A number of authors attribute such modulation to defects in the anion distribution because they also occur both in some pure calcites[14] and in calcites with impurities stemming from compositional variations.[44] Other modulations parallel to $10\bar{1}4$ have been described,[1] which would place the origin during special replacement growth conditions, in which a secondary carbonate replaces a primary molecule by dissolution reprecipitation across a thin film of aqueous solution.

Two Year Calcite. The HRTEM observations of a rhombohedral calcite crystal that developed in solution B (Figure 1k) in association with acicular aragonite revealed several defects (Figure 6). The atomic periodicity was indicative of the presence of Moiré fringes around the $[1\bar{1}00]$ zone axis. The optical diffractions for OR1, OR2, and OR3 (Figure 6b,c,d, respectively) confirmed the presence of several orientations. The alignment and lattice mismatch could be calculated from the Moiré fringes. The Moiré pattern is formed by the intersection of several sets of atomic rows in planes 0006 and $11\bar{2}3$. OR1 exhibited the 0006 atomic planes whose respective fft's (Figure 6b) suggest the presence of defects, as shown by the streaking associated with the 0006 reflection. OR2 exhibited columns of 0006 and $11\bar{2}3$ atoms. The stacking sequence misfit indicates movements in the columns of atoms (Figure 6a). Several Burgers vectors can be identified on the lattice image. The stacking sequence exhibited fringe displacement with $1/3d_{11\bar{2}3\text{calcite}}$ spacing. The dislocation strain field was generated by the presence of extra spots associated with 0006 (arrows in the fft). These spots were formed by two defects that caused extrastructural periodicity as observed in real space. OR3 exhibited Moiré fringes affecting 0006, as confirmed by the fft (Figure 6d). The interfacial stresses in the 2 year sample may be the result of a mismatch generated by differences in hydration/dehydration conditions.

The Effect of High Relative Humidity. The interpretation of HRTEM images can identify certain characteristics induced by the environment to which the colloidal solutions of portlandite nanocrystals were exposed. Since neoformed crystals of the two $CaCO_3$ polymorphs nucleated and grew in precursor alcoholic solutions exposed to a high humidity environment (75% RH), differences in the water/alcohol ratio very likely modified the local parent structure. These minor irregularities were reflected in the existence of defects such as observed here.

Under high relative humidity conditions, water significantly affects calcium carbonate polymorph stability, inducing structural defects that may give rise to dislocations and the generation of hydrated polymorphs.[30] Such observations readily show that the presence, position, orientation, and density of this kind of defect impact calcite crystal local structure and stability, modifying its reactivity and mechanical properties.[1] The presence of water around the surface favors the introduction of point defects, enlarging the dislocation network and generating other defects. There is evidence that under high relative humidity conditions, a surface tension and capillary force related contraction in the cell parameter over time[30] may contribute to the generation of this kind of structure, due to the rise in cohesive energy.[47] Differences in the stress energy may generate residual stress fields induced by elastic energy stored in the crystal or in the dislocation network, where energy is concentrated inside grains. The latter is regarded as one of the main driving forces behind recrystallization. The stored energy associated with residual stress may also affect this process, however.[48] This behavior has been observed in particle aggregation, where dislocations, stacking faults, and grain boundaries are generated. In particular, if surface nanoparticles are chemically altered, for example, passivated by a thin coating of water or surfactant, or if their composition or stoichiometry is modified, dense agglomerations of defects may be preserved

dx.doi.org/10.1021/cg300628m | *Cryst. Growth Des.* 2012, 12, 4844−4852

at grain boundaries during aggregation.[49] These defects may govern the physical properties of the aggregate, while kinetic factors determine its stability. Grain boundary density and structure are also important factors in aggregate recrystallization. The energy furnished by such defects may drive diffusion and recrystallization.[50] H_2O is known to enhance the rates of both intracrystalline and grain boundary diffusion and therefore to facilitate dislocations and diffusion-accommodated creep.[51] This effect may acquire considerable importance when water is released during dehydration or carbonation reactions. A number of mechanisms come into simultaneous play in dehydration, including grain boundary diffusion due to the presence of dehydration water.[48]

Differences in defect microstructures might be related to rhythmic variations in humidity conditions, including the vapor pressure in the climatic chamber. These variations, which would affect calcite crystallization, would modify the equilibrium composition of the calcite−residual liquid pair and thus induce the defects displayed by the crystals. The appearance of a large number of irregularities would be associated with differences in growth, during which the liquid−solid interface would be particularly affected both by CO_2 and H_2O in the environment.

Exposure to high relative humidity entails a risk of irreversible changes in the surface area and structure during hydration/dehydration cycles. The dissolution process rearranges all the bonds in the exposed material, resulting in polymorphism, strains, or other defects.[1] Dissolution/recrystallization processes may involve hydration/dehydration reactions. The release of H_2O during carbonation would cause dehydration of calcium carbonate precursor phases, namely, ACC and monohydrocalcite, and their transformation into metastable polymorphs (ikaite), to subsequently give rise to anhydrous $CaCO_3$. Nucleation would begin in the least (vaterite and aragonite) and end in the most stable phase (calcite). If an excess of H_2O is released, more hydrated $CaCO_3$ could precipitate in successive cycles as CO_2 is taken up into the carbonate crystal lattice.

The initial surface of the $Ca(OH)_2$ transformed into $CaCO_3$ is continuously modified by any adsorbed H_2O not completely removed during hydration/dehydration cycles. The surface energies of the previously formed hydrated polymorphs (monohydrocalcite)[29,30] and neoformed metastable aragonite or vaterite (which may reappear) are modified by the chemisorption of H_2O. During long-term carbonation, the precursor nanoparticles are surrounded by saturation or adsorbed water. The surfaces of the particles must therefore adjust to bonding with water molecules and possibly excess or surplus protons depending on the pH. This alone may cause a significant difference in the nature of the particle surface relative to a dry surface or one exposed to a dry atmosphere.[50] Furthermore, long-range periodic symmetry is broken, affecting bonding orbital systems and vibrational states and with them many aspects of the spectroscopic signature.[50]

The amount of structural defects such as dislocations in calcite neoforming during solution A carbonation and the existence of stacking faults in solution B denoted obvious differences in crystal stability. Some of these differences not only were exposure time related but may also have been related to starting solution conditions and possible environmental changes (primarily variations in RH, temperature, pH, surface tension, or CO_2 concentration). The 35-day calcite exhibited modulated structures, which have been associated with structural distortions.[52] These structures are ordinarily metastable, resulting from reactions that have not yet reached completion. They often provide information about precursor phases and reaction mechanisms.[53] The study of dislocations in carbonates has been vital to the evaluation of their dissolution mechanisms.[54]

CONCLUSIONS

Lattice defects observed at a resolution of 1.7 Å contribute to clarifying aragonite to calcite transformation. These defective structures are the result of the uptake of CO_3^{2-} in the lattice, with the release of H_2O. The resulting stress fields induce the formation of dislocations and stacking faults, favoring aragonite to calcite phase transformation. The defects appearing in the aragonite lattice include stacking faults, the insertion of extra atomic planes in the normal lattice sequence, and vacancies. Both extra atoms and nanoporosity confirm the involvement of crystallization/dissolution processes. Calcite nucleation mechanisms are the result of the rearrangement of CO_3 anions in areas where disorder is generated by dislocations in the aragonite lattice. The atomic defects observed in both aragonite and calcite can be applied to predict the solubility behavior of these polymorphs under high relative humidity conditions. The differences between the two solutions with respect to crystalline habit, crystal size, aggregation, and type of atomic scale structural defects may be expected to affect the polymorphic properties of $CaCO_3$ and in particular carbonation kinetics under the experimental conditions described here.

AUTHOR INFORMATION

Corresponding Author

*E-mail: luzgomez@geo.ucm.es.

Funding

The present research was funded by the Autonomous Community of Madrid under its GEOMATERIALES program (S2009/MAT-1629), the Spanish Ministry of Science and Innovation under the Consolider-Ingenio 2010 program (CSD2007-0058), and the Complutense University of Madrid research group, Alteration and Conservation of heritage stone materials (ref 921349).

Notes

The authors declare no competing financial interest.

ACKNOWLEDGMENTS

The authors are grateful to the anonymous referees, from whose constructive criticism and suggestions this paper has benefitted. Thanks go as well to Professor Alejandro Varez for his comments and suggestions. Margaret Clark is acknowledged for her assistance with the English text.

REFERENCES

(1) Wenk, H. R.; Barber, D. J.; Reeder, R. In *Carbonates: Mineralogy and Chemistry*; Reeder, R., Ed.; Reviews in Mineralogy; Mineralogical Society of America: Washington, DC, 1990; Vol. *11*, pp 301−367.

(2) Parsonage, N. G.; Staveley, L. A. K. *Disorder in Crystals*; Oxford University Press: New York, 1978.

(3) Carlson, W. In *Carbonates: Mineralogy and Chemistry*; Reeder, R., Ed.; Reviews in Mineralogy; Mineralogical Society of America: Washington, DC, 1990; Vol. *11*, pp 191−225.

(4) Liu, M.; Yund, R. A. *Contrib. Mineral. Petrol.* **1993**, *114*, 465−478.

(5) Liu, R.; Xu, X.; Cai, Y.; Cai, A.; Pan, H.; Tang, R.; Cho, K. *Cryst. Growth Des.* **2009**, *9*, 3095−3099.

(6) Didymus, J.; Young, J. R.; Mann, S. *Proc. R. Soc. London* **1994**, *258*, 237−245.

(7) Huang, Z.; Zhang, G. *Cryst. Growth Des.* **2012**, *12*, 1816−1822.
(8) Falini, G.; Albeck, S.; Weiner, S.; Addadi, L. *Science* **1996**, *271*, 67−69.
(9) Benzerara, K.; Menguy, N.; Obst, M.; Stolarski, J.; Mazur, M.; Tylisczak, T.; Brown, G. E., Jr.; Meibom, A. *Ultramicroscopy* **2011**, *111*, 1268−1275.
(10) Chevalier, N. R.; Chevallard, C.; Goldmann, M.; Brezesinski, G.; Guenoun, P. *Cryst. Growth Des.* **2012**, *12*, 2299−2305.
(11) Hayashi, A.; Nakamura, T.; Watanabe, T. *Cryst. Growth Des.* **2010**, *10*, 5085−5091.
(12) Sarikaya, M.; Fong, H.; Sopp, J. M.; Katti, K. S.; Mayer, G. *15th ASCE Engineering Mechanics Conference*; Columbia University: New York, 2002; http://www.civil.columbia.edu/em2002/proceedings/papers/595.pdf
(13) Barber, D. J.; Wenk, H. R. In *Electron Microscopy in Mineralogy*; Wenk, H. R., Ed.; Springer-Verlag: Berlin, 1976; pp 428−422.
(14) Gunderson, S. H.; Wenk, H. R. *Am. Mineral.* **1981**, *66*, 789−800.
(15) Barber, D. J.; Wenk, H. R. *Eur. J. Mineral.* **2001**, *13*, 221−243.
(16) O'Keefe, M. A.; Barber, D. J. *Int. Phys. Conf. Ser.* **1984**, *68*, 177−180.
(17) Reeder, R. In *Minerals and Reactions at the Atomic Scale: Transmission Electron Microscopy*; Buseck, P., Ed.; Reviews in Mineralogy; Mineralogical Society of America: Washington, DC, 1992; Vol. *27*, pp 381−424.
(18) Aquilano, D.; Bruno, M.; Massaro, F. R.; Rubbo, M. *Cryst. Growth Des.* **2011**, *11*, 3985−3993.
(19) Bruno, M.; Massaro, F. R.; Prencipe, M.; Aquilano, D. *CrystEngComm* **2010**, *12*, 3626−3633.
(20) Akiyama, T.; Nakamura, K.; Ito, T. *Phys. Rev. B* **2011**, *84*, No. 085428.
(21) Tendeloo, V.; Gronsky, W. *Phys Chem. Minerals* **1985**, *12*, 333−341.
(22) Pokroy, B.; Fitch, A. N.; Zolotoyabko, E. *Cryst. Growth Des.* **2007**, *7*, 1580−1583.
(23) Aquilano, D.; Rubbo, M.; Catti, M.; Pavese, A. *J. Cryst. Growth* **1997**, *182*, 168−184.
(24) Thiery, M.; Villain, G.; Dangla, P.; Platret, G. *Cem. Concr. Res.* **2007**, *37*, 1047−1058.
(25) Dickinson, S. R.; Henderson, G. E.; McGrath, K. M. *J. Cryst. Growth* **2002**, *244*, 369−378.
(26) Plummer, L. N.; Wigley, T. M. L.; Parkhurst, D. L. *Am. J. Sci.* **1978**, *278*, 179−216.
(27) Ashurst, J.; Dimes, F. G. In *Conservation of Building and Decorative Stone*; Butterworth-Heinemann: London, 1990; Vol. *2*, pp 169−184.
(28) Rodriguez-Navarro, C.; Ruiz-Agudo, E.; Ortega-Huertas, M.; Hansen, E. *Langmuir* **2005**, *21*, 10948−10957.
(29) López-Arce, P.; Gomez-Villalba, L. S.; Martínez-Ramirez, S.; Álvarez de Buergo, M.; Fort, R. *Powder Technol.* **2011**, *205*, 263−269.
(30) Gomez-Villalba, L. S.; López-Arce, P.; Alvarez de Buergo, M.; Fort, R. *Appl. Phys. A: Mater. Sci. Process.* **2011**, *104*, 1249−1254.
(31) López-Periago, A. M.; Pacciani, R.; Vega, L. F.; Domingo, C. *Cryst. Growth Des.* **2010**, *10*, 4823−4830.
(32) Gomez-Villalba, L. S.; López-Arce, P.; Fort, R. *Appl. Phys. A: Mater. Sci. Process.* **2012**, *106*, 213−217.
(33) Sand, K. K.; Rodriguez-Blanco, J. D.; Makovicky, E.; Benning, L. G.; Stipp, S. L. S. *Cryst. Growth Des.* **2012**, *12*, 842−853.
(34) Mosharraf, M.; Sebhatu, T.; Nyström, C. *Int. J. Pharm.* **1999**, *177*, 29−51.
(35) Rodriguez-Navarro, C.; Ruiz-Agudo, E.; Luque, A.; Rodriguez-Navarro, M.; Ortega-Huertas, L. *Am. Mineral.* **2009**, *94*, 578−593.
(36) Wenk, H. R.; McTigue, J. W. In *Proceedings of the Seventh International Conference on High Voltage Electron Microscopy*; Fisher, R. M., Gronsky, R., Westmacot, K. H., Eds.; Lawrence Berkeley Laboratory University of California: Berkeley, California, U.S.A., 1983; pp 347−352.
(37) Momma, K.; Izumi, F. J. *Appl. Crystallogr.* **2011**, *44*, 1272−1276.
(38) Aquilano, D.; Costa, E.; Genovese, A.; Massaro, F. R.; Pastero, L.; Rubbo, M. *J. Cryst. Growth* **2003**, *247*, 516−522.
(39) Nabarro, F. R. N.; Quintanilha, A. T. In *Dislocations in Solids*; Nabarro, F. R. N., Ed.; North-Holland Publishing Co.: New York, 1980; Vol. *5*, p 223.
(40) Perdikouri, C.; Kasioptas, A.; Geisler, T.; Schmidt, B.; Putnis, A. *Geochim. Cosmochim. Acta* **2011**, *75*, 6211−6224.
(41) Reeder, R. In *Carbonates: Mineralogy and Chemistry*; Reeder, R., Ed.; Reviews in Mineralogy; Mineralogical Society of America: Washington DC, 1990; Vol. *11*, pp 1−47.
(42) Dal Negro, A; Ungaretti, I. *Am. Mineral.*. **1971**, *56*, 768−772.
(43) Maslen, E. N.; Streltsov, V. A.; Streltsova, N. R. *Acta Crystallogr.* **1993**, *B49*, 636−641.
(44) Frisia-Bruni, S.; Wenk, H. R. *J. Sediment. Res* . **1985**, *55* (2), 159−170.
(45) Baronnet, A. In *Minerals and Reactions at the Atomic Scale; Transmission Electron Microscopy*; Buseck, P., Ed.; Reviews in Mineralogy; Mineralogical Society of America: Washington, DC, 1992; Vol. *27*, pp 277−278.
(46) Alnheck, C.; Zeografi, G. *Int. J. Pharm.* **1990**, *62*, 87−95.
(47) Khanna, S. N.; Bucher, J. P.; Buttet, J.; Cyrot-Lackman, F. *Surf. Sci.* **1983**, *127*, 165−174.
(48) Baczmański, A.; Wierzbanowski, K.; Lipiński, P.; Bacroix, B.; Lodini, A. *J. Neutron Res.* **2007**, *15*, 281−287.
(49) Pen, R. L.; Banfield, J. F. *Science* **1998**, *281*, 969−971.
(50) Waychunas, G. A. *Rev. Mineral. Geochem.* **2001**, *44*, 105−166.
(51) Rubie, D. C. In *Deformation Process in Minerals, Ceramics and Rocks*; Barber, D. J., Meredith, P. G., Eds.; The Mineralogical Society Series: Springer, Unwin Hyman: London, 1990; pp 262−295.
(52) Buseck, P. R.; Cowley, J. M. *Am. Mineral.* **1983**, *68*, 18−40.
(53) Busseck, P.; Weblen, D. In *High Resolution Transmission Electron Microscopy and Associated Techniques*; Buseck, P., Cowley, J., Eyring, L., Eds.; Oxford University Press: New York, 1992; pp 308−377.
(54) MacInnis, I. N.; Brantley, S. L. *Geochim. Cosmochim. Acta* **1992**, *56*, 1113−1126.